



ELSEVIER

Journal of Electron Spectroscopy and Related Phenomena 94 (1998) 187–194

JOURNAL OF
ELECTRON SPECTROSCOPY
and Related Phenomena

Valence band photoemission and near-edge core excitation spectroscopy of di-*t*-butylchlorophosphine

C.W. Hutchings^a, A.P. Hitchcock^{b,*}, A.T. Wen^b, S.-D. Hwang^a, J.A. Glass^c, J.T. Spencer^c,
Y.-F. Hu^d, G.M. Bancroft^d, P.A. Dowben^{a,c}

^aDepartment of Physics and Astronomy and Center for Materials Research and Analysis, University of Nebraska, Lincoln, NE 68588-0111, USA

^bDepartment of Chemistry, McMaster University, Hamilton, L8S 4M1, Canada

^cDepartment of Chemistry and the W.M. Keck Center for Molecular Electronics, Syracuse University, Syracuse, NY 13244, USA

^dDepartment of Chemistry, University of Western Ontario, London, N6A 3K7, Canada

Received 1 December 1997; accepted 27 January 1998

Abstract

The electronic structure of di-*t*-butylchlorophosphine [(*t*-butyl)₂PCl] has been studied by photoemission spectroscopy (PES) and inner-shell electronic spectroscopy. The photoemission spectrum of (*t*-butyl)₂PCl exhibits features in good agreement with molecular orbital assignments based on modified neglect of differential overlap semiempirical calculations. The unoccupied electronic structure of (*t*-butyl)₂PCl has been investigated through P 2p, P 2s, Cl 2p, and C 1s core excitation spectra recorded by dipole-regime inner shell electron energy loss spectroscopy (ISEELS). The P 2p and P 2s spectra of (*t*-butyl)₂PCl exhibit features in common with PCl₃ and P(CH₃)₃, whereas the Cl 2p spectrum resembles that of PCl₃ and the C 1s spectrum resembles P(CH₃)₃. Comparison of the photoemission and the ISEELS results emphasizes the local structural sensitivity of core excitation in contrast to the more extended picture of electronic structure provided by PES. © 1998 Elsevier Science B.V. All rights reserved

Keywords: Core excitation; Photoemission; Di-*t*-butylchlorophosphine; Organometallic CVD

1. Introduction

Organophosphorus compounds, such as isobutylphosphine, *tert*-butylphosphine and other organometallic molecules, have been studied as substitutes for PH₃ in organometallic vapor phase epitaxy [1–3]. Such phosphorus-containing organometallic compounds are used in the fabrication of III-V materials and as source molecules for introducing phosphorus as a dopant [4]. Such organometallic compounds could, in principal, be tailored so as to improve

processing conditions and the surface chemical reactions involved in the vapor deposition process. Di-*t*-butylchlorophosphine [(*t*-butyl)₂PCl] is a potential phosphorus source which has not been previously explored for organometallic vapor phase epitaxy applications. Understanding radiation-induced decomposition pathways requires a detailed understanding of the occupied and unoccupied molecular orbital assignments in the vicinity of the chemical potential.

This paper compares experimental photoemission spectroscopy (PES) results of gas-phase (*t*-butyl)₂PCl with modified neglect of differential overlap (MNDO) semiempirical calculations. We also present inner

* Corresponding author

shell electron energy loss spectroscopy (ISEELS) measurements of gas-phase (t-butyl)₂PCl and compare the spectra with previously reported ISEELS spectra of gas-phase PCl₃ and P(CH₃)₃ [5]. PES samples the occupied levels, whereas ISEELS probes the unoccupied electronic structure in the region of the HOMO–LUMO gap.

2. Experimental

Gas-phase He I_α photoelectron spectroscopy of (t-butyl)₂PCl was undertaken on a McPherson ESCA-36 photoelectron spectrometer equipped with a hemispherical electrostatic analyzer and a hollow cathode UV helium lamp as described elsewhere [6]. The Ar 3p_{3/2} photoelectron line was used as an internal calibration source during data acquisition, and the resolution of the system was measured at 0.03 eV FWHM using Ar 3p_{3/2}. An He I_α source was used to produce 21.22 eV photons and all measurements are referenced to the vacuum level. (t-Butyl)₂PCl was admitted to the gas chamber through a leak valve and all measurements were taken at room temperature. Photoelectron spectra were fitted to a symmetric Lorentzian–Gaussian line shape to identify the vertical ionization energies (IP) [7].

The inner shell electron energy loss (ISEEL) spectrometer and its operation have been described in detail elsewhere [8,9]. ISEEL spectra were obtained by inelastically scattering a high velocity incident electron beam ($E_0 = 2.6$ – 2.8 keV) with di-t-butylchlorophosphine vapor. In order to achieve adequate vapor pressure of the source compound in the collision region of the spectrometer, the sample cell, inlet line, and collision chamber were heated. The scattering angle was $\sim 2^\circ$, and the instrumental resolution was 0.7 eV FWHM.

Molecular orbital (MO) calculations were performed using version 6.00 of MOPAC¹ [12] and follow MNDO semiempirical MO methods described elsewhere [13–15]. The orbital assignments of the calculated energy levels of the molecule are expressed in the point group symmetry C_s . We have assigned the

¹The parameterizations used for MNDO calculations were from Refs. [10,11].

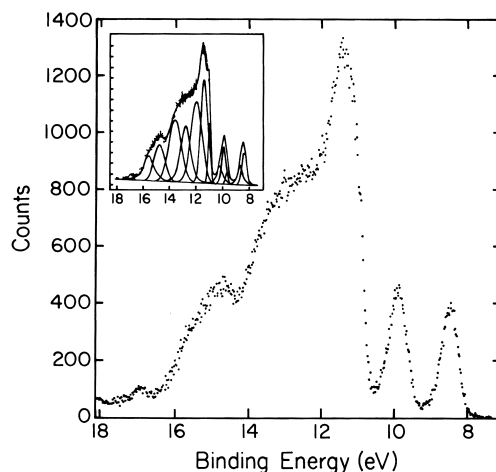


Fig. 1. Photoelectron spectrum of gaseous di-t-butylchlorophosphine [(t-Bu)₂PCl]. The inset shows a Lorentzian–Gaussian fit to aid peak identification and accurate measurement of the binding energies of photoemission peaks which are listed in Table 1.

photoemission features by assuming that the one-electron approximation holds and that the photoemission process follows Koopman's theorem [16,17]. This application of a ground state MO calculation to a final state spectroscopy is clearly an oversimplification. Nonetheless, this method of MO assignment is very effective, so long as the many-body effects result in a rigid relaxation shift for all MOs.

3. Photoemission: The occupied MOs

The photoemission spectrum of gaseous (t-butyl)₂-PCl is shown in Fig. 1. The inset shows the best fit of the individual photoemission features using a Lorentzian–Gaussian line shape. According to this fit there are 13 photoemission features from 8 to 17 eV binding energy (–8 to –17 with respect to the vacuum level). The results of the ground-state MNDO calculations and the measured values of the photoemission features are compared in Table 1. The difference between the calculated and measured values ($\Delta = \text{MNDO} - \text{measured binding energy}$) is consistently about -1.7 ± 0.2 eV. This shows the calculated MOs are in good agreement with experiment at low binding energy from approximately –10 to –15 eV with respect to the vacuum level. For calculated binding energies greater than 16 eV, comparison between

Table 1

MNDO calculated MO energies, observed binding energies, and observed core excitation term values for gaseous di-*t*-butylchlorophosphine

MO	Orbital energy (eV) MNDO ^a	Expt. energy (eV) ISEELS/UPS	Δ (eV)
19''	3.33	-2.4	5.6
19'	3.32		
18''	3.27		
18a'	3.21		
17a'' P-C	1.63	-3.5	5.1
17a' P-Cl/P-C	-0.56	-6.4	5.7
16a' P-Cl (LUMO)	-0.74		
15a' P-Cl (HOMO)	-10.14	-8.5	-1.6
16a'' Cl-P-C	-11.49	-9.8	-1.7
15a'' Cl-C	-12.58	-11.0	-1.6
14a' Cl-C	-12.60		
14a'' C-C	-12.64		
13a' Cl-C	-12.79	-11.3	-1.5
13a'' Cl-C	-12.95		
12a' Cl-P	-13.08		
12a''	-13.44	-11.9	-1.7
11a''	-13.46	-12.8	-1.5
11a'	-13.68		
10a''	-13.83		
9a''	-13.93		
10a'	-13.96	-13.5	-1.9
9a'	-14.30		
8a''	-15.08		
7a''	-15.16	-14.7	-1.5
6a''	-15.19		
8a'	-15.60	-15.6	-0.5
7a'	-16.11		
5a''	-16.21	-16.9	-2.1
6a'	-18.95		

^a The binding energies are relative to the vacuum level, and all values are in electron-volts.

^b Δ = MNDO-measured binding energy.

the MNDO calculation and the measured value of binding energy cannot be reconciled by a rigid final state relaxation shift. This is typical of ground-state MNDO calculations and may be related to limitations of the P and Cl basis sets used. MNDO has problems particularly when applied to assigning features associated with complex ion final states. Nonetheless, we have sufficient agreement between theory and experiment to assign the lower binding energy photoemission features.

The highest occupied MO (HOMO), 15a', which is primarily σ (P-Cl) character, is assigned to the photoemission feature at -8.5 eV. The photoemission feature at -9.8 eV is the 16a'' MO which results from the Cl-P-C molecular backbone. The photoemission feature

at -11.0 eV is the result of three MOs which are quite delocalized with density on both Cl and the *t*-butyl ligand.

Plots of the MNDO calculations for the HOMO (15a'), the lowest unoccupied MO (LUMO, 16a'), the LUMO + 1 (17a') and the LUMO + 2 (17a'') MOs are given in Fig. 2. The 16a' LUMO, which is mainly σ^* (P-Cl) in character, is calculated by MNDO to lie at -0.74 eV with respect to the vacuum level. (Note that the label σ^* (A-B) is not a valid symmetry designation; rather, it is used to give a qualitative sense of the orientation of the main electron density with respect to specific bonds). The 17a' LUMO + 1 has a mixed σ^* (P-C) and σ^* (P-Cl) character. In the ground state, the MNDO calculation predicts it occurs

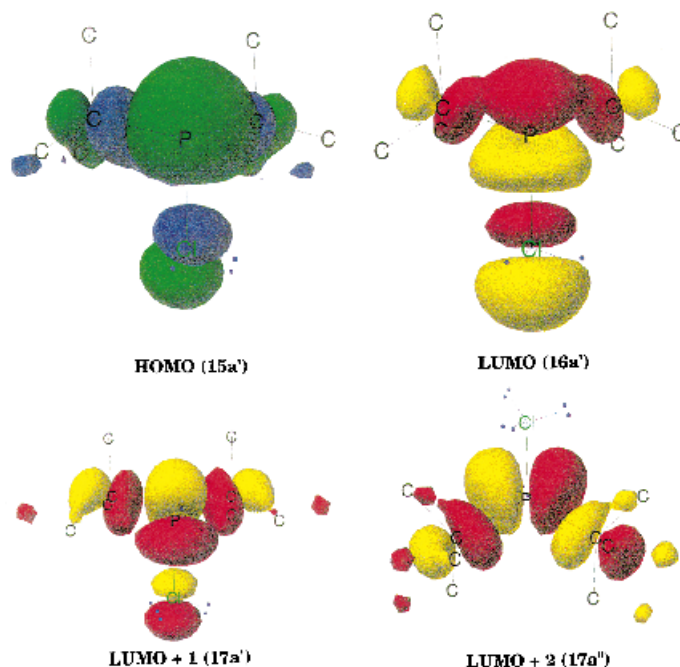


Fig. 2. Plots of the 15a' HOMO, the 16a' LUMO, the 17a' LUMO + 1 and the 17a'' LUMO + 2, all calculated using MNDO.

at -0.56 eV, only slightly higher in energy than the 16a' LUMO. MNDO places the 17a'' LUMO + 2, which has a dominant $\sigma^*(\text{P}-\text{C})$ character, at almost 2 eV higher energy. Core excitations to the 16a', 17a' and 17a'' orbitals are considered to be most important in explaining the low energy regions of the ISEELS data, as outlined in Section 4.

4. ISEELS measurements: The unoccupied MOs

The inner-shell excitation spectra of gaseous (t-butyl)₂PCl in the regions of P 2p, P 2s, Cl 2p, and C 1s excitation are presented in Figs 3–6. For comparison, Figs 4–6 also include high-resolution (0.18 eV FWHM) spectra of P(CH₃)₃ and PCl₃ taken from Ref. [5]. Energies, term values and proposed assignments are summarized in Table 2.

Fig. 3 shows an overview of the energy loss spectrum of (t-butyl)₂PCl between 100 and 300 eV. Fig. 4 shows the ISEELS spectra for the P 2p region of (t-butyl)₂PCl, P(CH₃)₃, and PCl₃. The P 2p spectrum of PCl₃ has been discussed by several authors

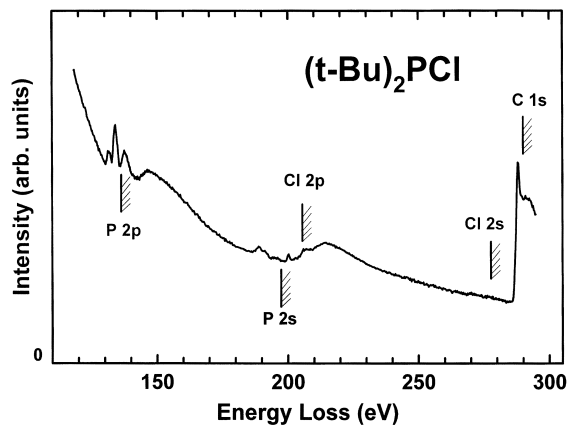


Fig. 3. Long-range electron energy loss spectrum (ISEELS) of (t-Bu)₂PCl covering the regions of P 2p, P 2s, Cl 2p, Cl 2s and C 1s excitation. The spectrum was recorded using 2.5 keV final electron energy (2.6–2.8 keV impact energy), 2° scattering angle and 0.7 eV FWHM energy resolution. The hatched lines give the locations of the indicated core IPs as estimated from the IPs of analogous species ([18]—see footnote to Table 2).

Table 2
Energies, term values and proposed assignments of features in the core excitation spectra of (t-butyl)₂PCl

#	Energy (eV)	Term value (eV) 2p _{3/2}	2p _{1/2}	Assignment
P 2p				
1 sh	131.2	6.4 ^e	—	(16a') σ*(P–Cl)
2	131.8	—	6.7 ^e	(16a') σ*(P–Cl)
3	133.9 ^a	3.7 ^e	—	(17a'') σ*(P–C)
IP(3/2) ^d	137.6	—	—	—
IP(1/2) ^d	138.5	—	—	—
4	141.0	—	—	—
5	158(2)	—	—	—
P 2s				
1	188.9(3)	—	6.1	16' σ*(P–Cl), 17a'' σ*(P–Cl, P–C)
2	191.0(3)	—	4.0	17' σ*(P–C)
IP ^d	195.0	—	—	—
3	196	—	—	—
Cl 2p				
1	200.1 ^b	6.3 ^e	—	(16 and 17a') σ*(P–Cl)
2	202.8	—	5.3 ^e	(16 and 17a') σ*(P–Cl)
3	204.1	2.3 ^e	—	(18 and 19a', a'')
4	206.0	—	2.1 ^e	(18 and 19a', a'')
IP(3/2) ^d	206.4	—	—	—
IP(1/2) ^d	208.1	—	—	—
5	207.5	—	—	—
6	216.6(8)	—	—	—
Cl 2s				
1	271.0(5)	—	6.6	16' σ*(P–Cl)
IP ^d	277.6	—	—	—
2	276.8(8)	—	—	—
C 1s				
1	286.9	—	3.5	(17a'') σ*(P–C); σ*(C–H)
2	288.05 ^c	—	2.4	18 and 19a'a'', σ*(C–H)
3 sh	289.5	—	0.9	—
IP ^d	290.4	—	—	—
3	291.4	—	—	—
4	292.6(5)	—	—	—
5 br	301(2)	—	—	—

^a Calibration: P 2p: –156.8(1) eV relative to CO₂ (290.74);

^b Calibration: Cl 2p: –88.0(1) eV relative to discrete C 1s signal = (288.05);

^c Calibration: C 1s: –2.68(6) relative to CO₂;

^d Ionization potentials estimated from XPS of similar species [22] as:

P 2p_{3/2}: PCl₃ (140.2); MePCl₂ (138.9) (therefore R₂PCl ~ 137.6 eV);

P 2s–P 2p_{3/2} average shift = 57.4 eV [5];

Cl 2p_{3/2}: PCl₃ (206.5); N₃P₃MeCl₅ (P–Cl 206.3);

Cl 2s–Cl 2p_{3/2} average shift = 71.2 eV [22];

C 1s: PMe₃ (290.3); isobutane (290.5).

^e 2p_{3/2} 2p_{1/2}.

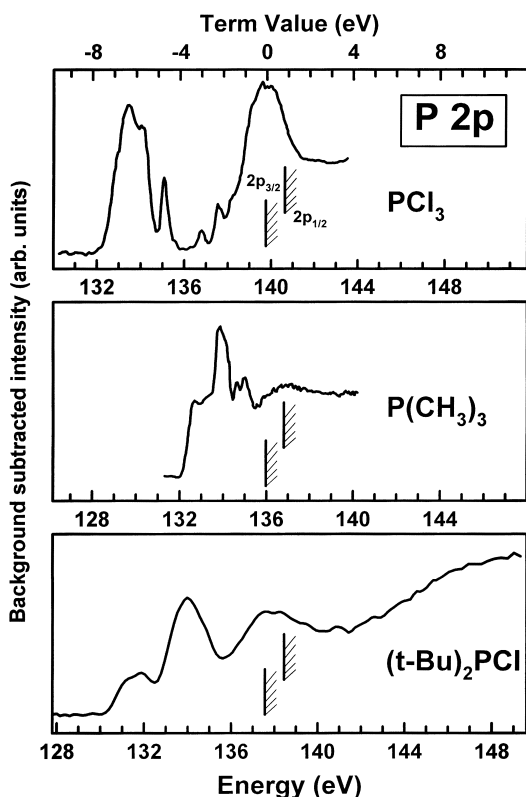


Fig. 4. Comparison of ISEEL spectra of $(t\text{-Bu})_2\text{PCl}$ of this work with those of PCl_3 and $\text{P}(\text{CH}_3)_3$ [5] in the P 2p region. The spectra are presented using energy scales shifted relative to each other in order to align at the P 2p IP (common term value scale). A curved background has been subtracted to isolate the P 2p signal. See caption to Fig. 3 for experimental details.

[5,8,19–22]. The lowest energy region of the P 2p spectrum of PCl_3 is the overlap of several states involving P 2p $\rightarrow \sigma^*(\text{P}-\text{Cl})$ transitions. The sharp single line at 135.4 eV is actually a dipole-forbidden, quadrupole-allowed transition to a $\{\text{P } 2p^{-1}, \sigma^*(\text{P}-\text{Cl})\} A_2$ state [5]. P 2p spectra of PCl_3 recorded by X-ray absorption do not show this feature [21,23]. A number of sharp Rydberg transitions then follow from 136 eV up to the P 2p_{3/2} IP at 140 eV. The strong broad feature at the continuum onset may be a low-lying shape resonance associated with the P 3d orbital, analogous to the S 3d-related (S 2p⁻¹, t_{2g}) state just above threshold in SF₆ [24]. The P 2p features of $\text{P}(\text{CH}_3)_3$ from 132 to 136 eV consist of many overlapping transitions which are not easily assigned [5], but which likely involve

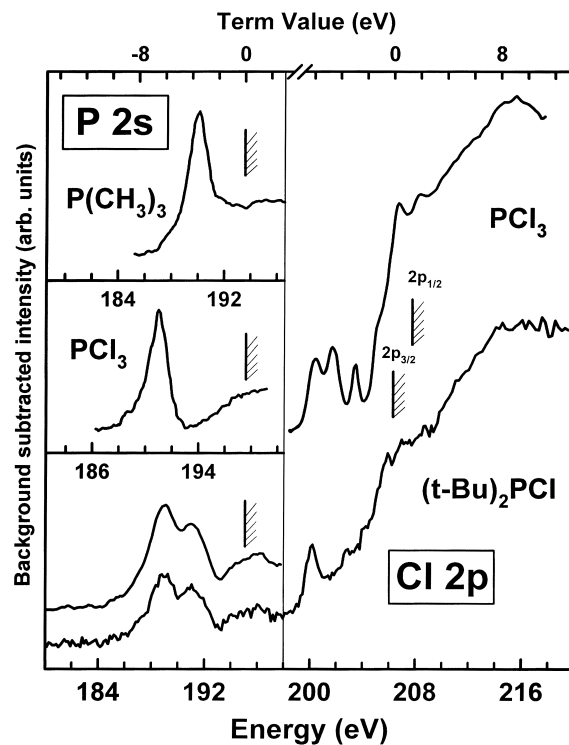


Fig. 5. Comparison of ISEELS spectra of $(t\text{-Bu})_2\text{PCl}$ of this work with those of PCl_3 and $\text{P}(\text{CH}_3)_3$ [5] in the P 2s region and that of PCl_3 in the Cl 2p region. The P 2s spectra are presented using energy scales shifted relative to each other in order to align at the P 2s IP (common term value scale). In each case a curved background has been subtracted to isolate the plotted signal. See caption to Fig. 3 for experimental details.

states of both $\sigma^*(\text{P}-\text{C})$ and Rydberg character. The P 2p spectrum of $(t\text{-butyl})_2\text{PCl}$ shows features common to both PCl_3 and $\text{P}(\text{CH}_3)_3$. Note that the P 2p spectra have been plotted in Fig. 4 on a common term value scale (TV = IP - E), i.e. the energy scale of each plot has been selected to align the P 2p_{3/2} IP, as determined by XPS, or estimated from values for similar species [25] (see footnotes to Table 2). A similar approach has been used to plot the P 2s spectra in Fig. 5. This approach is often helpful in revealing corresponding spectral features in related molecules, since term values are often similar for transitions from different core levels to a final level of similar spatial distribution and binding energy [5]. With this alignment the lowest energy feature in $(t\text{-butyl})_2\text{PCl}$ at 131 eV aligns reasonably well on the term value

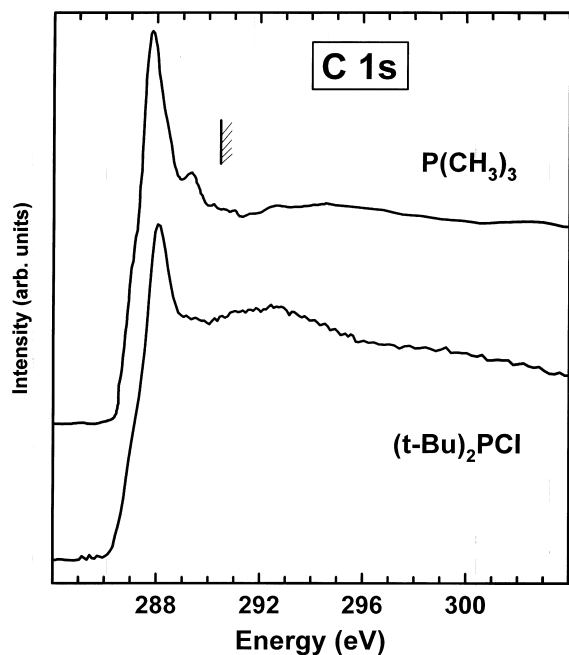


Fig. 6. Comparison of ISEELS spectra of (t-Bu)₂PCl of this work with that of P(CH₃)₃ [5] in the C 1s region. In each case a curved background has been subtracted to isolate the C 1s signal. See caption to Fig. 3 for experimental details.

scale with the lowest energy, broad $\sigma^*(\text{P}-\text{Cl})$ band in PCl₃. Similarly, although with less precision, the band at 138 eV in (t-butyl)₂PCl aligns on the term value scale with the lowest energy P 2p transition of P(CH₃)₃, which is likely of $\sigma^*(\text{P}-\text{C})$ character. On this basis we propose that the broad 138 eV band in (t-butyl)₂PCl is associated with several, unresolved P 2p $\rightarrow \sigma^*(\text{P}-\text{C})$ transitions. We do not expect as much Rydberg state contribution in (t-butyl)₂PCl as observed in either PCl₃ or P(CH₃)₃, on account of the much larger ligands. The lowest energy P 2p excitation in (t-butyl)₂PCl is expected to be the P 2p_{3/2} \rightarrow 16a', $\sigma^*(\text{P}-\text{Cl})$ excitation. Since the 16a' orbital has mainly P 3p and little P 2s or P 3d character (see Fig. 2), the transition is expected (and observed) to be quite weak in the dipole-regime ISEEL spectrum.

Fig. 5 shows the P 2s ISEEL spectra for all three species and the Cl 2p spectra of (t-butyl)₂PCl and PCl₃. On the common term value presentation of Fig. 5, it is very clear that the first band seen in the P 2s spectrum of (t-butyl)₂PCl directly correlates with the single band in the P 2s spectrum of PCl₃ (of

$\sigma^*(\text{P}-\text{Cl})$ character) and the second band directly correlates with the single band in the P 2s spectrum of P(CH₃)₃ (of $\sigma^*(\text{P}-\text{C})$ character). Thus we assign the lowest excitation at 189 eV (TV \sim 6 eV) to overlap of P 2s \rightarrow LUMO, (16a', $\sigma^*(\text{P}-\text{Cl})$) and P 2s \rightarrow LUMO + 1, (17a', $\sigma^*(\text{P}-\text{Cl}, \text{P}-\text{C})$) transitions, and the second band at 192 eV (TV \sim 4 eV) to P 2s \rightarrow LUMO + 2, (17a'', $\sigma^*(\text{P}-\text{C})$) transitions. It would be interesting to measure the relative intensity of these two lines in the P 2s spectrum of the intermediate species, (t-butyl)PCl₂. If these states really do reflect a local bonding character one would expect the 189 eV peak to grow relative to the 192 eV peak.

Since the Cl 2p IP of PCl₃ and (t-butyl)PCl₂ are similar, we have plotted the Cl 2p spectra on the same energy scale in Fig. 5. The features at 200.1 and 202.8 eV in PCl₃ are attributed to the spin-orbit components of Cl 2p $\rightarrow \sigma^*(\text{P}-\text{Cl})$ excitations [5]. By analogy, we attribute the 200–202 eV signal in the Cl 2p spectrum of (t-butyl)PCl₂ to Cl 2p \rightarrow 16a', $\sigma^*(\text{P}-\text{Cl})$ and Cl 2p \rightarrow 17a', $\sigma^*(\text{P}-\text{Cl})$ transitions. The feature at 204.1 eV may also have contributions from Cl 2p excitations to unoccupied valence MOs, although weak Rydberg contributions are also expected in this energy region. We do not expect to see any signal from Cl 2p \rightarrow 17a'' excitation since the 17a'' MO has no density on chlorine (see Fig. 2).

Fig. 6 shows the C 1s ISEEL spectra of (t-butyl)₂PCl (this work) and P(CH₃)₃ (from Ref. [5]). The lowest energy band is attributed in part to overlapping C 1s \rightarrow 17a', $\sigma^*(\text{P}-\text{Cl}, \text{P}-\text{C})$ and C 1s \rightarrow 17a'', $\sigma^*(\text{P}-\text{C})$ transitions, although the dominant contribution is likely C–H resonances at the methyl carbon atoms of the (t-butyl) groups, with perhaps some 3s and 3p Rydberg character. C 1s excitations to the 16a' LUMO are not expected since this orbital has mainly $\sigma^*(\text{P}-\text{Cl})$ character with little contribution from C 2p orbitals. The majority of the signal in the C 1s spectrum of (t-butyl)₂PCl is associated with the carbon atoms of the t-butyl group. For this reason the spectrum is quite similar to that of isobutane [18] and other saturated hydrocarbons.

5. Summary

The lower energy features in the inner shell spectra (ISEELS) of (t-butyl)₂PCl exhibit many features in

common with the corresponding core level spectra of PCl_3 and $\text{P}(\text{CH}_3)_3$, once core level energy shifts are taken into account. This allows us to conclude that the low energy unoccupied MOs are spatially localized in all three species. MNDO calculations of the ground state of $(t\text{-butyl})_2\text{PCl}$ reproduce the spatially localized character of the unoccupied levels. The core excitation term values are shifted lower by about 5.5 eV with respect to the calculated ground-state unoccupied orbital energies on account of the Coulombic interaction with the core hole.

The photoemission spectrum was assigned with the assistance of the MNDO calculations. The ground-state calculation of the binding energies of the low-lying occupied MOs are rigidly shifted by $-1.7(2)$ eV relative to the measured binding energies. From our comparisons with both PES and ISEELS we conclude that the MNDO results correctly predict the ordering and nature of the unoccupied and occupied MOs near the gap.

Acknowledgements

This work was funded by the Air Force Office of Scientific Research through grant #F49620-94-1-0433, the W.M. Keck Center for Molecular Electronics and the Center for Materials Research and Analysis.

References

- [1] C.H. Chen, C.A. Larsen, G.B. Stringfellow, *J. Cryst. Growth* 77 (1986) 11.
- [2] R. Karlicek, J.A. Long, V.M. Donnelly, *J. Cryst. Growth* 68 (1984) 123.
- [3] G. Laube, U. Kohler, J. Weidlein, F. Scholz, K. Streubel, R.J. Dieter, N. Karl, M. Gerdon, *J. Cryst. Growth* 93 (1988) 45.
- [4] S.-D. Hwang, P.A. Dowben, A. Cheeseman, J.T. Spencer, D.N. McIlroy, in: R.W. Collins, P.M. Fauchet, I. Shimizu, J.-C. Vial, T. Shimida, A.P. Alivisatos (Eds.), *Advances in Microcrystalline and Nanocrystalline Semiconductors*, MRS Symposium Proceedings, vol. 452, 1997, pp. 1031–1036.
- [5] R.N.S. Sodhi, C.E. Brion, *J. Electron Spectrosc. Relat. Phenom.* 37 (1985) 97.
- [6] L.L. Coatsworth, G.M. Bancroft, D.K. Creber, R.J. Lazier, P.W.M. Jacobs, *J. Electron Spectrosc. Relat. Phenom.* 13 (1978) 395.
- [7] G.M. Bancroft, J. Adams, L.L. Coatsworth, C.D. Bennewitx, J.D. Brown, W.D. Westwood, *Anal. Chem.* 47 (1975) 586.
- [8] A.P. Hitchcock, *Phys. Scripta T* 31 (1990) 159.
- [9] A.P. Hitchcock, S. Bealieu, T. Steel, F. Stohr, *J. Chem. Phys.* 80 (1980) 3927.
- [10] M.J.S. Dewar, M.L. McKee, *J. Chem. Soc.* 99 (1977) 5231.
- [11] M.J.S. Dewar, W.J. Theil, *J. Am. Chem. Soc.* 99 (1977) 4899.
- [12] J.J.P. Stewart, F.J. Seiler, *Quantum Chem. Program Exchange*, No 549.
- [13] S. Lee, D. Li, P.A. Dowben, F.K. Perkins, M. Onellion, T.J. Spencer, *J. Am. Chem. Soc.* 113 (1991) 8444.
- [14] J.A. Glass, T.A. Whelan, J.T. Spencer, *Organometallics* 10 (1991) 1161.
- [15] R.W. Miller, K.J. Donaghy, J.T. Spencer, *Organometallics* 10 (1991) 1148.
- [16] W.L. Jolly, in: C.R. Brundle, A.D. Baker (Eds.), *Electron Spectroscopy: Theory, Techniques and Applications*, vol. 1, Academic Press, London, 1977, Chapter 3, p. 119.
- [17] R.E. Ballard, *Photoelectron Spectroscopy and Molecular Orbital Theory*, Adam Hilger, 1978.
- [18] A.P. Hitchcock, I. Ishii, *J. Electron Spectrosc.* 42 (1987) 11.
- [19] I.A. Topol, A.V. Kondratenko, L.N. Mazalov, *Opt. Spectrosc.* 50 (1981) 267.
- [20] I.A. Topol, A.V. Kondratenko, L.N. Mazalov, *Bull. Acad. Sci. USSR Phys. Ser.* 46 (1982) 143.
- [21] E. Ishiguro, S. Iwata, A. Mikuni, Y. Suzuki, H. Kanamon, T. Sasaki, *J. Phys. B: At. Mol. Phys.* 20 (1987) 4725.
- [22] J.W. Au, C.E. Brion, *Chem. Phys.* 218 (1997) 87.
- [23] A. Jurgensen, R.G. Cavell, N. Kosugi, J. Neville, A.P. Hitchcock, in preparation.
- [24] J.T. Francis, C.C. Turci, T. Tylliszczak, G.G.B. de Souza, N. Kosugi, A.P. Hitchcock, *Phys. Rev. A* 52 (1995) 4665.
- [25] W.L. Jolly, K.D. Bomben, C.J. Eyer mann, *At. Data Nucl. Data Tables* 31 (1984) 433.